Published in final edited form as:
J Tissue Eng Regen Med. 2009 August ; 3(6): 477–485. doi:10.1002/term.188.

Characterization of Engineered Tissue Construct Mechanical Function by Magnetic Resonance Imaging

C. P. Neu[1,2,†], **H. F. Arastu**[2], **S. Curtiss**[2], and **A. H. Reddi**[2]

[1] Weldon School of Biomedical Engineering, Purdue University, West Lafayette, IN, 47907-2032

[2] Center for Tissue Regeneration and Repair, University of California, Davis, Medical Center, Sacramento, CA 95817

Abstract

Noninvasive magnetic resonance imaging (MRI) is a technology that enables the characterization of multiple physical phenomena in living and engineered tissues. Mechanical function of engineered tissues is a primary endpoint for the successful regeneration of many biological tissues such as articular cartilage, spine, and heart. Here, we demonstrate the application of MRI to characterize mechanical function of engineered tissue. Phase contrast-based methods were demonstrated to characterize detailed deformation fields throughout the interior of native and engineered tissue using an articular defect model as a study system. MRI techniques revealed that strain fields varied nonuniformly depending on spatial position. Strains were highest in the tissue constructs compared to surrounding native cartilage. Tissue surface geometry corresponded to strain fields observed within the tissue interior near the surface. Strain fields were further evaluated with respect to the spatial variation in concentrations of glycosaminoglycans ([GAG]), critical proteoglycans in the extracellular matrix of cartilage, as determined by gadolinium-enhanced imaging. [GAG] concentration also varied nonuniformly depending on spatial position and was lowest in the tissue constructs compared to the surrounding cartilage. The use of multiple MRI techniques to assess tissue mechanical function provide complementary data and suggest that deformation is related to tissue geometry, underlying extracellular matrix constituents, and the lack of tissue integration in the model system studied. Specialized and advance MRI phase contrast-based methods are valuable for the detailed characterization and evaluation of mechanical function of tissue engineered constructs.

Keywords

Magnetic Resonance Imaging (MRI); Mechanical Characterization; Functional Construct Analysis; Elastography; Defect Model; Articular Cartilage

1. INTRODUCTION

Magnetic resonance imaging (MRI) is a noninvasive experimental technique that is capable of characterizing multiple physical phenomena in living tissue (Haacke et al. 1999). Classical measures of parameters such as spin density and relaxation rates (e.g. T_1 and T_2) characterize morphology and the local nature of interacting protons and molecules. Other MRI methods permit the separation of water and fat signals in spatially localized tissue regions as well as the calculation of magnetization transfer, diffusion, and flow.

[†]Corresponding Author: Tel: (765) 496-1426, Fax: (765) 494-0902, cpneu@purdue.edu.

MRI has been used to assess tissue engineered constructs for the replacement and regeneration of diseased or damaged tissue. A functional assessment of meniscal cartilage included measurements of perfusion and flow in a bioreactor system for the optimization of tissue properties (Neves et al. 2003). Integration of articular cartilage with a hydrated polymer gel was investigated using T_2 as a measure of effectiveness (Ramaswamy et al. 2006). Additional studies further utilized T_2 measures (Watrin-Pinzano et al. 2004; Terrovitis et al. 2006; Chesnick et al. 2007), magnetization transfer (Chesnick et al. 2007), T_1 measures with contrast agents (Marolt et al. 2006), and $T_{1\rho}$ measures and sodium imaging (Novotny et al. 2006).

For tissues that provide a primarily mechanical role in the body, specialized and advanced MRI-based techniques are required to characterize regenerative medicine strategies in terms of mechanical function. Articular cartilage is one particular tissue that is critical to the normal function of human synovial joints. The tissue has unique mechanical and tribological properties that allows for locomotion by providing a low friction and load bearing joint surface. The breakdown in cartilage function is observed in osteoarthritis, a debilitating disease associated with progressive cartilage degradation and altered joint mechanics (i.e. deformation in response to applied loads). There has been limited success to regenerate articular cartilage through the application of tissue engineering technologies (Reddi 1998), although considerable promise remains (Hettrich et al. 2008).

MRI-based methods to evaluate cartilage function include measures of tissue deformation and extracellular matrix concentrations. Tissue deformation measures through the 3D volume of cartilage are based on tag registration (Neu et al. 2005) and phase contrast (Neu and Walton 2008) methods. These techniques provide a local measure of deformation to a high (e.g. 0.17% strain) precision. The dGEMRIC (Delayed Gadolinium-Enhanced MRI of Cartilage) technique provides spatial information of glycosaminoglycan (GAG) content using T_1-relaxation time measurements after penetration of the hydrophilic contrast agent Gd-DTPA^{2-} (Bashir et al. 1999). The measure of [GAG] by dGEMRIC correlates with surface measures of mechanical stiffness (Samosky et al. 2005) and has additionally been used to evaluate degenerated, developing, and repaired cartilage (Gray et al. 2007).

The purpose of this study was to demonstrate the use of a specialized MRI-based tissue deformation method for the functional and mechanical evaluation of engineered tissue. An articular cartilage full thickness defect was simulated using a bovine explant model system. An acute defect was made and repair simulated using chondrocyte-laden agarose constructs cultured in the presence or absence of serum or growth factors. Function was evaluated in terms of strain fields computed throughout the cartilage-agarose construct. The strain fields observed were related to the underlying extracellular matrix content as evaluated by gadolinium-enhanced imaging methods.

2. METHODS

2.1. Hydrogel Constructs

Articular chondrocytes extracted from native articular cartilage were used in the creation of hydrogel constructs. Articular chondrocytes were acquired from 3 month-old bovine stifle (tibiofemoral) joints obtained within 6 hours of sacrifice from a local abattoir (Figure 1). Joints were opened under aseptic conditions to expose the femoral condyles. A scalpel was used to shave off the top 2–3 mm from the medial and lateral condyles. After rinsing the tissue slices with PBS containing antibiotic solution, full thickness chondrocytes were isolated by digestion with 0.2% collagenase-P (Roche Pharmaceuticals, Nutley, NJ) for 5 hours (Luyten et al. 1994). Isolated chondrocytes in monolayer cultures were plated at a high density (1×10^6 cells/ml) in 10 cm diameter culture plates. For monolayer cultures, cells

were placed in chemically-defined low glucose Dulbecco's modified Eagle medium: nutrient mixture F12 (Ham) 1:1 (D-MEM/F-12, Invitrogen), supplemented with 0.1% bovine serum albumin, 100 units/ml penicillin, 100μg/ml streptomycin, 50μg/ml ascorbate-2-phosphate, and 10% fetal bovine serum (FBS; Invitrogen, Carlsbad, CA). Cells were expanded over one week and one passage to confluency.

Hydrogel constructs were created using agarose and articular chondrocytes. Agarose was specifically chosen for this simple model system (to demonstrate the MRI deformation method) considering the high water content of cartilage tissue (accounting for more than 80% of the wet tissue weight at the surface and 65% in the deep zone (Mow et al. 1992)) and the ability to vary the construct stiffness depending on the agarose concentration. Chondrocytes were released from culture plates using a brief (<3–5 min) 0.25% trypsin-EDTA (Invitrogen) digestion, rinsed, and then mixed with low-melt agarose (Bio-Rad Laboratories, Hercules, CA) for a final concentration of 2% agarose and 5×10^6 cells/ml. Full thickness (5 mm) cylindrical constructs were removed from the cured agarose-chondrocyte mix using a coring reamer (8 mm diameter, Fisher Scientific).

2.2. Defect Model and Experiments

Hydrogel constructs were used to observe the influence of culture conditions and supplemental factors on tissue function. Hydrogel constructs were placed in individual wells of a 12-well culture plate (3 mL/well) and treated with chemically-defined media (described previously) and one of three culture conditions: serum-free (0% FBS), 10% FBS, or serum-free supplemented with 300 ng/ml recombinant human bone morphogenetic protein- (BMP-) 7 (generously provided by Dr. David Rueger, Stryker Biotech, Hopkinton, MA). Long-term culture was maintained for a period of 35 days with replacement of culture medium and appropriate supplements every 2–3 days.

On the day of the functional MRI analysis, *cartilage repair constructs* were created using the hydrogel constructs and fresh osteochondral explants. The cartilage repair construct was a simulated *in vitro* model for the repair of an acute cartilage defect (Buckwalter and Mankin 1998). The **four** cartilage repair constructs investigated were: (a) *0% FBS model*, (b) *10% FBS model*, and (c) *BMP-7 model*, all created using the hydrogel constructs described previously, as well as (d) *replaced cartilage model*, created by removing and then immediately replacing the cylindrical plug cut from the cartilage explant. Importantly, the 0% and 10% FBS samples were used to replicate standard cell and organ culture systems for articular cartilage (e.g. (Khalafi et al. 2007)). The BMP-7 model was chosen considering bone morphogenetic proteins promote new cartilage and bone growth (Reddi 1998; Reddi 2002). The replaced cartilage model served as a positive control samples in the analysis of GAG content. Additionally, a *no cells model* was created using an additional set of hydrogel constructs without embedded cells. Since the *no cell model* system did not undergo 35 days of culture, data from this model system was used to demonstrate field data (Figures 3 and 5A), but was not used for comparison to other constructs. Briefly, a 5 mm thick cartilage explant was removed using a coring reamer (8 mm diameter, Fisher Scientific) from the lateral femoral condyles (Figure 1). An acute full-thickness defect was created using a 3 mm coring reamer in the center and through the depth of the explant. A cut (3 mm diameter) hydrogel construct or replaced cartilage was inserted (press-fit) into the surrounding explant. The cartilage repair constructs were placed in chemically-defined medium for up to three hours. The culture time for cartilage repair constructs was sufficiently short to limit construct and explant integration which was expected to manifest in tissue-level deformation patterns. At the time of testing, constructs were affixed to delrin mounts using ethyl cyanoacrylate and placed in an MRI-compatible bioreactor (described subsequently). A successful repair for this model system was defined as the functional restoration of the hydrogel construct or replaced cartilage to levels of the surrounding explant tissue.

2.3. MRI-Compatible Bioreactor

An MRI-compatible bioreactor was designed to allow for mechanical loading within the MRI scanner in addition to fluid exchange for biochemical studies. The bioreactor was configured for use in a vertical bore 400 MHz MR imaging system (9.4 Tesla, Bruker Medical GMBH, Ettlingen Germany) (Figure 2). Mechanical loading was accomplished using a servo pressure regulator to drive a double-acting and low friction (i.e. carbon fiber piston on glass) pneumatic cylinder. This configuration allowed for load-controlled compression cycles to be applied to constructs with millisecond timing precision (Neu et al. 2005). Biochemical studies (e.g. those requiring fluid exchange and the introduction of MRI contrast agents) were accomplished using tubing extending into sample holder at the magnet isocenter. Syringes were used to exchange fluid while maintaining the sample orientation and position which facilitated registration of spatially-dependent biochemical data during time-course experiments.

2.4. Functional MRI Analysis: Tissue Deformography

Displacements through the cartilage repair construct volume were determined during cyclic compressive loading using a custom MRI pulse sequence (Neu and Walton 2008). The imaging plane was chosen as the slice through the center of the cartilage repair construct. Briefly, tissue displacements were determined using displacement-encoding by stimulated echo (DENSE; (Aletras et al. 1999)) and fast spin echo (FSE) pulse sequences. Key DENSE parameters were: t_{enc} = 1.0 ms, G_{de} =100 mT/m for in-plane displacement encoding, and G_{de} =0 mT/m for the reference image. FSE imaging parameters were: TR = 3000 ms; TE = 6.05 ms; number of echoes per excitation = 16; in-plane spatial resolution = 100 × 100 μm^2; image matrix size = 256 × 256 $pixels^2$; number of averages = 4; slice thickness = 1.0 mm.

Timing integration of the MRI-compatible bioreactor mechanical actions with the DENSE-FSE sequence was implemented to reduce motion artifacts due to cyclic loading (Figure 2). Imaging was accomplished such that phase encode steps were acquired over many loading cycles. Phase cycling of the second rf pulse (+cosine, -cosine, +sine, and –sine modulation (Epstein and Gilson 2004)) was also accomplished to eliminate artifacts due to FSE readout and ultimately used to isolate the single displacement-encoded echo by image processing. During each 3 s cycle, the mechanical load of 15.6 N was applied to the constructs for a total of 1.5 s. The replaced cartilage model sample was additionally tested at 27.4 N to visualize the mechanical integration between the cut cartilage surfaces. These loading conditions resulted in an average normal stress (normalizing to the 8 mm cartilage repair construct diameter) of 0.3 and 0.5 MPa, respectively, acting through the loading platen to the articular surface. To prevent blurring of images due to any changes in the deformation of the cartilage between load cycles, images were acquired only after the cartilage reached a steady state load-displacement response during the unconfined compressive cyclic loading applied by the loading apparatus (Neu and Hull 2003).

Custom image processing software determined construct deformations in MATLAB (v.6.0, The Mathworks, Natick, MA) (Neu and Walton 2008). The phase-cycled data sets were combined for artifact elimination (Epstein and Gilson 2004), and a 2D inverse Fourier transform was applied to the combined raw data to determine phase images (i.e., reference, *x*- and *y*-displacement encoded images). Phase images were unwrapped and displacements were determined by subtracting *x*- and *y*-displacement encoded images from the reference image. The Green-Lagrange strain tensor was computed from displacement data. Strain in the loading direction (E_{yy}) and transverse directions (E_{xx}), as well as shear strains (E_{xy}) were computed as a function of position directly as components of the strain tensor.

Strain fields were visualized for one sample of each of the treatment groups described previously. To aide in image processing and visualization, undeformed and deformed images were additionally acquired using an FSE sequence with an in-plane spatial resolution of 100 × 100 μm^2. Subsequent to image acquisition, a deformed image of cartilage was segmented manually using software employing closed Bezier curves to identify arbitrary object shapes within images (Paravision 3.0, Bruker Medical GMBH, Ettlingen, Germany) and used as an image mask in the previously described image processing steps to isolate the tissue from surrounding bathing solution.

2.5. Functional MRI Analysis of Glycosaminoglycans

The concentration of glycosaminoglycans ([GAG]), critical proteoglycans in the extracellular matrix of cartilage, was determined with the delayed gadolinium-enhanced MRI of cartilage (dGEMRIC) technique. Importantly, use of the custom bioreactor with fluid exchange and mechanical loading capabilities allowed for immediate registration and superposition of cartilage displacement and [GAG] data, i.e. [GAG] was determined in the same imaging plane as that described previously for tissue deformography. Briefly, T_1 measurements were made using a saturation recovery pulse sequence (TR = 100, 200, 400, 800, 1600, 3200 ms) before and after the implementation of 2 mM Gd-$DTPA^{2-}$ (Magnevist, Berlex Laboratories, Wayne, NJ). Constructs were then equilibrated for more than 5 hours following exchange of PBS with PBS + Gd-$DTPA^{2-}$ to allow for complete diffusion of the contrast agent into the tissue volume (Bashir et al. 1999). Conversion of T_1 field data to [GAG] was determined following the standard method (Bashir et al. 1999). Computation of calibration coefficient R (sec/mM) was determined using T_1 measurements of graded Gd-$DTPA^{2-}$ standards (0.2 – 2.0 mM, in increments of 0.2 mM). For the 400 MHz MR imaging system and 25 °C sample experimental temperature, R = 4.49 sec/mM. Relative [GAG] (i.e. construct [GAG]/surrounding cartilage [GAG]) was determined for one sample of each treatment group using all points in the imaging plane representing the tissue type of interest. Results are presented as the mean ± one standard deviation and are representative of the variation in relative [GAG] of pixels within the single sample investigated.

3. RESULTS

Deformation fields in the tissue-engineered constructs during simple cyclic compressive loading were nonuniform and depended on spatial location (Figures 3 and 4). Displacements in the loading direction (d_y) of the no cells model sample approached – 160 μm near the agarose-indentor boundary and 0 μm near the agarose-base boundary (Figure 3A). Prior to cyclic loading, the articular surface of the cartilage and agarose were flush (white arrow with black head). During the undeformed portion of each loading cycle, the agarose surface contained irregularities (e.g. protrusions and gaps) compared to the surrounding cartilage (solid white arrow), and thus deformed to a higher magnitude. The same pattern was observed in the BMP-7 and 10% FBS model samples where agarose surface irregularities resulted in higher measured displacements (solid white arrow; Figures 4C and 4D). In the 0% FBS model sample (Figure 4B), a flush articular surface was observed between the agarose and cartilage during the unloading period of each cycle, and the measured displacements in the loading region were of less magnitude compared to other treatment groups. In the replaced cartilage model sample (Figure 4A), increasing the applied load resulted in a more pronounced mechanical mismatch in displacements between cut cartilage surfaces (solid black arrow).

Gadolinium-enhanced imaging of tissue constructs enabled calculation of tissue fixed charge density and [GAG] that also varied by spatial position (Figure 5A). [GAG] was similar in the replaced cartilage model tissue, but near zero in the hydrogel construct of the no cells model sample (Figure 4A). Tissue contrast between hydrogel construct and the surrounding

cartilage and bathing solution was minimal in proton density-weighted and T_1 (pre-Gd(DTPA)$^{2-}$) images. Importantly, [GAG] content was not restored to that of surrounding cartilage in any group except the Replaced Cartilage sample (Figure 4B).

4. DISCUSSION

The aim of this study was to demonstrate the use of magnetic resonance imaging to evaluate the function of tissue engineered cartilage constructs. Function was evaluated in an articular cartilage defect model in terms of displacement fields computed throughout the tissue construct. Primary results in this study were (1) deformation fields varied nonuniformly depending on spatial position, (2) strains were highest in the hydrogel constructs compared to surrounding cartilage, and (3) [GAG] was lowest in the hydrogel constructs compared to the surrounding cartilage. This work represents the first application of the DENSE-FSE technique to engineered cartilage and in combination with techniques for biochemical assessment such as dGEMRIC.

The ability to measure *in situ* tissue quality is essential for assessing the success of cartilage repair techniques. Current techniques for measuring tissue quality include optical coherence tomography (Han et al. 2003) and photoacoustic (Ishihara et al. 2005) techniques. Optical coherence tomography allows for the identification of subtle changes in tissue structure, including surface fibrillations comparable to histological analysis at low magnification. Photoacoustic measurements provide data regarding bulk viscoelastic relaxation times. In comparison, while the spatial resolution of images from the MRI techniques discussed herein does not approach the optical scale, the present technique provides spatially-resolved characterization of mechanical deformation with minimal error. The DENSE-FSE technique used herein has been demonstrated to exhibit minimal error, with zero bias and a displacement and strain precision of 8.8 μm and 0.17%, respectively. Thus, the technique is appropriate for characterizing tissue-level deformations noninvasively in engineered tissue.

There has been limited use of MRI to investigate mechanical function in the emerging fields of tissue engineering and regenerative medicine. Routinely, standard mechanical testing techniques have assessed bulk properties of engineered cartilage (e.g. (Hofmann et al. 2006)). Additionally, bulk properties have been shown to correlate with MRI parameters such as T_1, T_2, and the diffusion coefficient (Miyata et al. 2007). Only recently have MRI techniques been developed to assess and characterize tissue-level deformation patterns throughout the volume of the material under the application of physiologically-relevant mechanical loading (Neu and Walton 2008).

Precise timing of MRI actions was required. T_1 measures were taken prior to mechanical loading (pre-Gd(DTPA)$^{2-}$) and following the fluid exchange (post-Gd(DTPA)$^{2-}$) to ensure that tissue morphology was similar for the two sets of images. Differences in morphology (due to mechanical loading and tissue creep) would have precluded registration of T_1 measures and calculation of [GAG]. Also, the integration of cyclic loading and MRI pulse sequence actions was required for images free of motion artifacts (Neu and Hull 2003).

Strain fields in the hydrogel constructs were typically larger compared to those in the surrounding cartilage. The mismatch was attributed to at least three factors. First, there was a lack of GAGs in the repair tissue compared to the surrounding cartilage. Proteoglycans are known to contribute to the load support of cartilage through interactions with water in the highly hydrated tissue (Maroudas 1976). The lack of GAGs in the repair tissue may have not provided sufficient load support and resulted in increased deformations. Second, there were observed differences and variability in the morphology of unloaded tissue that corresponded to strain fields (Figure 4). Differences in material properties (e.g. creep under cyclic loading

or swelling behavior resulting from altered biochemical content) may have contributed to surface geometry irregularities. Thus, there is a need for appropriate matching of material properties for a successful repair. In the case of articular cartilage, the study of allograft or autograft tissues may be of interest considering the variation of tissue even within the same joint of an individual (Neu et al. 2007). Further studies with larger sample sizes are required to address these concerns. Third, the lack of integration in the model system resulted in alterations of the strain field data that depended on load (Figure 4A). Thus, the study of tissue integration is critical in future cartilage repair experiments.

The concentration of glycosaminoglycans in the hydrogel constructs was not restored to levels of the surrounding cartilage for the treatments investigated. The use of BMP-7 resulted in [GAG] that was lower compared to the use of 10% FBS-supplemented media. This finding may be attributed to the milieu of molecules present in serum that may include BMPs in addition to other morphogens and growth factors (Reddi 1998). Importantly, the heterogeneous biochemical composition of degenerated and repaired articular cartilage (Gray et al. 2007) has been explored and monitored using dGEMRIC both *in vitro* (e.g. (Allen et al. 1999)) and *in vivo* (e.g. (Trattnig et al. 2007)). Further, while the measurement of [GAG] using dGEMRIC has been directly validated versus the dimethylmethylene blue (DMMB) biochemical assay in human cartilage (Bashir et al. 1999), the use of the polar agarose hydrogel could have interfered with Gd-DTPA^{2-} actions and resulted in false positives (i.e. elevated relative [GAG]) in this tissue engineering application. Thus, for the application of dGEMRIC to measure [GAG] restoration in engineered cartilage, a careful consideration of the scaffold material is required in addition to the optimum type, concentration, and incubation period for media supplements. The general tissue engineering strategy for restoration of GAG concentrations will likely involve the novel combinations of cells, acellular biomaterials, drugs, gene products, or genes that may be designed, specified, fabricated, and delivered either simultaneously or sequentially as therapeutic agents (Boyce 2002).

Integration strategies are required to aide in distributing mechanical force from the repair to the surrounding tissue. The defect model used herein did not allow for tissue integration seen especially in the mismatch in strain fields (Figure 4). A model of successful repair is therefore required that is based on increasing incubation times or altering other parameters (e.g. use of growth factors or enzymatic pretreatments (Quinn and Hunziker 2002)) to allow for integration between the tissue surfaces. The application of the techniques described herein to an animal model (Chan et al. 2007) of a tissue repair would address the mechanical function of integrated tissues.

This study demonstrated the ability of MRI to noninvasively evaluate mechanical function in a defect repair model in tissue explants. In particular, strain fields were evaluated to a high precision. The technique in its current state is appropriate to analyze novel biomimmetic scaffolding materials alone or in combination with stem cells and inductive signals (e.g. morphogens, growth factors, or mechanical forces), and may readily be applied for study of natural or synthetic scaffolding-based constructs for cartilage repair. Regenerative success, defined in terms of deformation fields, and the integration of native tissue with allograft/autograft or other repair tissues, may be studied post-removal from the living organism. Further development of the techniques for use in (e.g. the whole joints of) animals or humans will require the appropriate development of MRI pulse sequences and methods for *in vivo* application of mechanical forces to normal, diseased, and regenerated tissue of interest.

Acknowledgments

Our study was funded by the National Institutes of Health (NIBIB 1F32 EB003371-01A1) and the Lawrence J. Ellison Endowed Chair.

References

Aletras AH, Ding S, Balaban RS, Wen H. DENSE: displacement encoding with stimulated echoes in cardiac functional MRI. J Magn Reson. 1999; 137(1):247–52. [PubMed: 10053155]

Allen RG, Burstein D, Gray ML. Monitoring glycosaminoglycan replenishment in cartilage explants with gadolinium-enhanced magnetic resonance imaging. J Orthop Res. 1999; 17(3):430–6. [PubMed: 10376734]

Bashir A, Gray ML, Hartke J, Burstein D. Nondestructive imaging of human cartilage glycosaminoglycan concentration by MRI. Magn Reson Med. 1999; 41(5):857–65. [PubMed: 10332865]

Boyce, ST. Regulatory Issues and Standardization. In: Atala, A.; Lanza, RP., editors. Methods of Tissue Engineering. San Diego, CA: Academic Press; 2002. p. 3-15.

Buckwalter JA, Mankin HJ. Articular cartilage repair and transplantation. Arthritis Rheum. 1998; 41(8):1331–42. [PubMed: 9704631]

Chan, DD.; Neu, CP.; Hull, ML. Tibiofemoral cartilage deformation determined in cyclic compression by displacement-encoded MRI. Transactions of the 54th Annual ORS Meeting; San Francisco, CA. 2007.

Chesnick IE, Avallone FA, Leapman RD, Landis WJ, Eidelman N, Potter K. Evaluation of bioreactor-cultivated bone by magnetic resonance microscopy and FTIR microspectroscopy. Bone. 2007; 40(4):904–12. [PubMed: 17174620]

Epstein FH, Gilson WD. Displacement-encoded cardiac MRI using cosine and sine modulation to eliminate (CANSEL) artifact-generating echoes. Magn Reson Med. 2004; 52(4):774–81. [PubMed: 15389939]

Gray ML, Burstein D, Kim YJ, Maroudas A. Magnetic resonance imaging of cartilage glycosaminoglycan: Basic principles, imaging technique, and clinical applications. J Orthop Res. 2007

Haacke, EM.; Brown, RW.; Thompson, MR.; Venkatesan, R. Magnetic Resonance Imaging: Physical Principles and Sequence Design. New York, NY: John Wiley & Sons, Inc; 1999.

Han CW, Chu CR, Adachi N, Usas A, Fu FH, Huard J, Pan Y. Analysis of rabbit articular cartilage repair after chondrocyte implantation using optical coherence tomography. Osteoarthritis Cartilage. 2003; 11(2):111–21. [PubMed: 12554127]

Hettrich CM, Crawford D, Rodeo SA. Cartilage repair: third-generation cell-based technologies -- basic science, surgical techniques, clinical outcomes. Sports Med Arthrosc. 2008; 16(4):230–5. [PubMed: 19011555]

Hofmann S, Knecht S, Langer R, Kaplan DL, Vunjak-Novakovic G, Merkle HP, Meinel L. Cartilage-like tissue engineering using silk scaffolds and mesenchymal stem cells. Tissue Eng. 2006; 12(10): 2729–38. [PubMed: 17518642]

Ishihara M, Sato M, Sato S, Kikuchi T, Mochida J, Kikuchi M. Usefulness of photoacoustic measurements for evaluation of biomechanical properties of tissue-engineered cartilage. Tissue Eng. 2005; 11(7–8):1234–43. [PubMed: 16144459]

Khalafi A, Schmid TM, Neu C, Reddi AH. Increased accumulation of superficial zone protein (SZP) in articular cartilage in response to bone morphogenetic protein-7 and growth factors. J Orthop Res. 2007; 25(3):293–303. [PubMed: 17143906]

Luyten FP, Chen P, Paralkar V, Reddi AH. Recombinant bone morphogenetic protein-4, transforming growth factor-beta 1, and activin A enhance the cartilage phenotype of articular chondrocytes in vitro. Exp Cell Res. 1994; 210(2):224–9. [PubMed: 8299720]

Marolt D, Augst A, Freed LE, Vepari C, Fajardo R, Patel N, Gray M, Farley M, Kaplan D, Vunjak-Novakovic G. Bone and cartilage tissue constructs grown using human bone marrow stromal cells, silk scaffolds and rotating bioreactors. Biomaterials. 2006; 27(36):6138–49. [PubMed: 16895736]

Maroudas AI. Balance between swelling pressure and collagen tension in normal and degenerate cartilage. Nature. 1976; 260(5554):808–9. [PubMed: 1264261]

Miyata S, Numano T, Homma K, Tateishi T, Ushida T. Feasibility of noninvasive evaluation of biophysical properties of tissue-engineered cartilage by using quantitative MRI. J Biomech. 2007; 40(13):2990–8. [PubMed: 17442320]

Mow VC, Ratcliffe A, Robin Poole A. Cartilage and diarthrodial joints as paradigms for hierarchical materials and structures. Biomaterials. 1992; 13(2):67–97. [PubMed: 1550898]

Neu CP, Hull ML. Toward an MRI-based method to measure non-uniform cartilage deformation: an MRI-cyclic loading apparatus system and steady-state cyclic displacement of articular cartilage under compressive loading. J Biomech Eng. 2003; 125(2):180–8. [PubMed: 12751279]

Neu CP, Hull ML, Walton JH. Heterogeneous three-dimensional strain fields during unconfined cyclic compression in bovine articular cartilage explants. J Orthop Res. 2005; 23(6):1390–8. [PubMed: 15972257]

Neu CP, Hull ML, Walton JH, Buonocore MH. MRI-based technique for determining nonuniform deformations throughout the volume of articular cartilage explants. Magn Reson Med. 2005; 53(2):321–8. [PubMed: 15678528]

Neu CP, Khalafi A, Komvopoulos K, Schmid TM, Reddi AH. Mechanotransduction of bovine articular cartilage superficial zone protein by transforming growth factor beta signaling. Arthritis Rheum. 2007; 56(11):3706–14. [PubMed: 17968924]

Neu CP, Walton JH. Displacement encoding for the measurement of cartilage deformation. Magn Reson Med. 2008; 59(1):149–55. [PubMed: 18050342]

Neves AA, Medcalf N, Brindle K. Functional assessment of tissue-engineered meniscal cartilage by magnetic resonance imaging and spectroscopy. Tissue Eng. 2003; 9(1):51–62. [PubMed: 12625954]

Novotny JE, Turka CM, Jeong C, Wheaton AJ, Li C, Presedo A, Richardson DW, Reddy R, Dodge GR. Biomechanical and magnetic resonance characteristics of a cartilage-like equivalent generated in a suspension culture. Tissue Eng. 2006; 12(10):2755–64. [PubMed: 17518645]

Quinn TM, Hunziker EB. Controlled enzymatic matrix degradation for integrative cartilage repair: effects on viable cell density and proteoglycan deposition. Tissue Eng. 2002; 8(5):799–806. [PubMed: 12459058]

Ramaswamy S, Wang DA, Fishbein KW, Elisseeff JH, Spencer RG. An analysis of the integration between articular cartilage and nondegradable hydrogel using magnetic resonance imaging. J Biomed Mater Res B Appl Biomater. 2006; 77(1):144–8. [PubMed: 16208691]

Reddi AH. Role of morphogenetic proteins in skeletal tissue engineering and regeneration. Nat Biotechnol. 1998; 16(3):247–52. [PubMed: 9528003]

Reddi, AH. Introduction. In: Hascall, VC.; Kuettner, KE., editors. The Many Faces of Osteoarthritis. Basel, Switzerland: Birkhauser Verlag; 2002. p. 63-66.

Samosky JT, Burstein D, Eric Grimson W, Howe R, Martin S, Gray ML. Spatially-localized correlation of dGEMRIC-measured GAG distribution and mechanical stiffness in the human tibial plateau. J Orthop Res. 2005; 23(1):93–101. [PubMed: 15607880]

Terrovitis JV, Bulte JW, Sarvananthan S, Crowe LA, Sarathchandra P, Batten P, Sachlos E, Chester AH, Czernuszka JT, Firmin DN, Taylor PM, Yacoub MH. Magnetic resonance imaging of ferumoxide-labeled mesenchymal stem cells seeded on collagen scaffolds-relevance to tissue engineering. Tissue Eng. 2006; 12(10):2765–75. [PubMed: 17518646]

Trattnig S, Marlovits S, Gebetsroither S, Szomolanyi P, Welsch GH, Salomonowitz E, Watanabe A, Deimling M, Mamisch TC. Three-dimensional delayed gadolinium-enhanced MRI of cartilage (dGEMRIC) for in vivo evaluation of reparative cartilage after matrix-associated autologous chondrocyte transplantation at 3.0T: Preliminary results. J Magn Reson Imaging. 2007; 26(4):974–82. [PubMed: 17896385]

Watrin-Pinzano A, Ruaud JP, Cheli Y, Gonord P, Grossin L, Bettembourg-Brault I, Gillet P, Payan E, Guillot G, Netter P, Loeuille D. Evaluation of cartilage repair tissue after biomaterial implantation in rat patella by using T2 mapping. Magma. 2004; 17(3–6):219–28. [PubMed: 15580373]

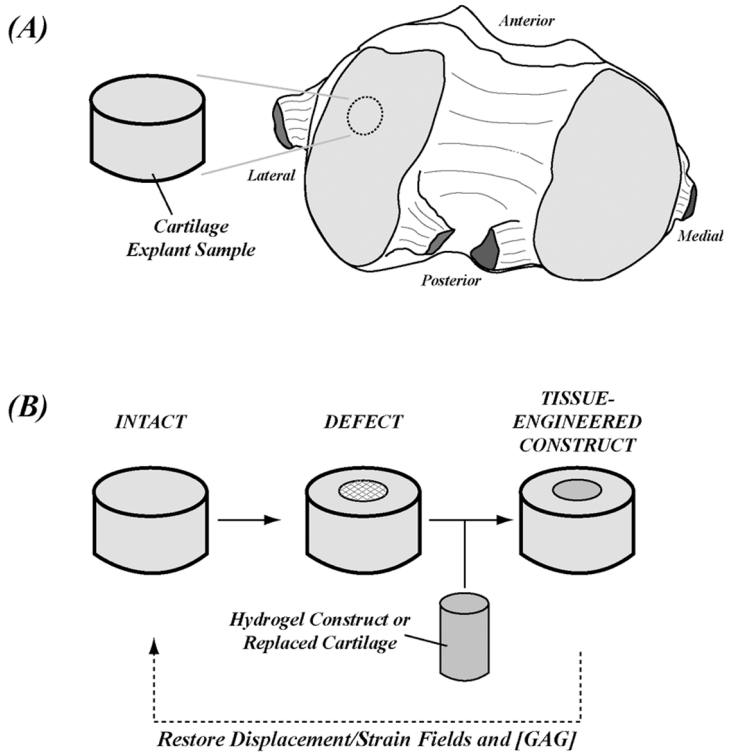

Figure 1.

MRI functional analyses of engineered tissues were conducted in an articular cartilage defect model as a study system. Harvest locations for intact explants were on the lateral femoral condyles in the load-bearing region *(A)*. A full-thickness and acute defect model was created in the articular cartilage and filled with a hydrogel construct that consisted of chondrocytes in agarose and media supplements *(B)*. The goal of a successful repair in the hydrogel construct was defined as the restoration of deformation fields in the construct compared to the surrounding native cartilage.

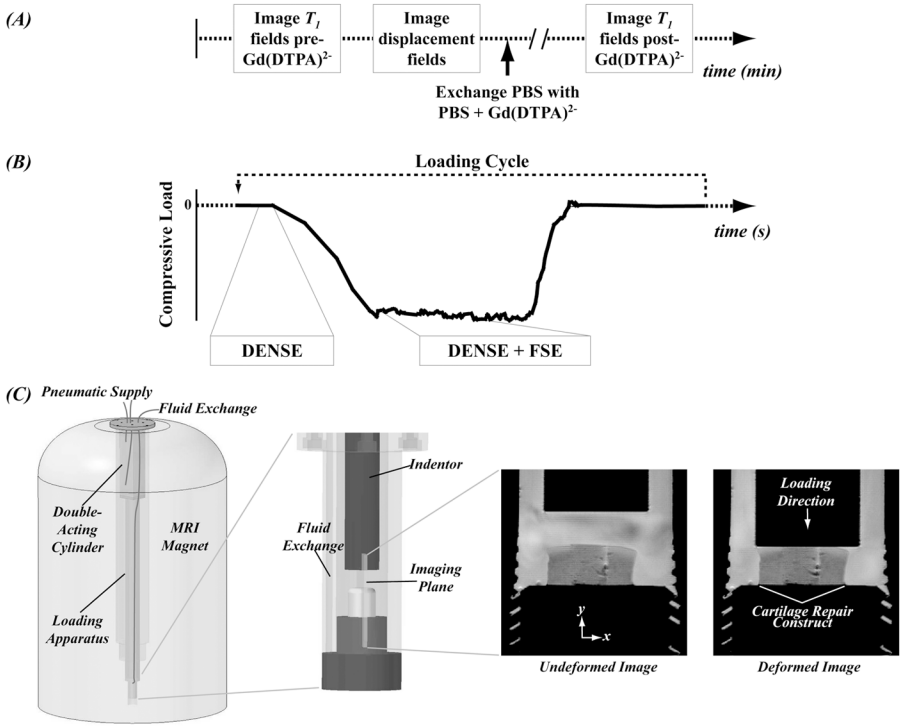

Figure 2.

Functional MRI analyses determined deformation and [GAG] fields in the tissue and required precise timing methods. Timing of fluid exchange actions, MRI T_1 measurements, and mechanical loading allowed for computation of deformation fields and [GAG] *(A)*. Integration of DENSE and FSE pulse sequences during cyclic mechanical loading allowed for measurement of deformation fields *(B)*. A custom MRI-compatible bioreactor was used for application of mechanical loading and fluid exchange *(C)*. Standard MRI (FSE alone) generated undeformed and deformed images with similar proton density in the construct and surrounding tissue and did not allow for functional assessment of the tissue-engineered construct.

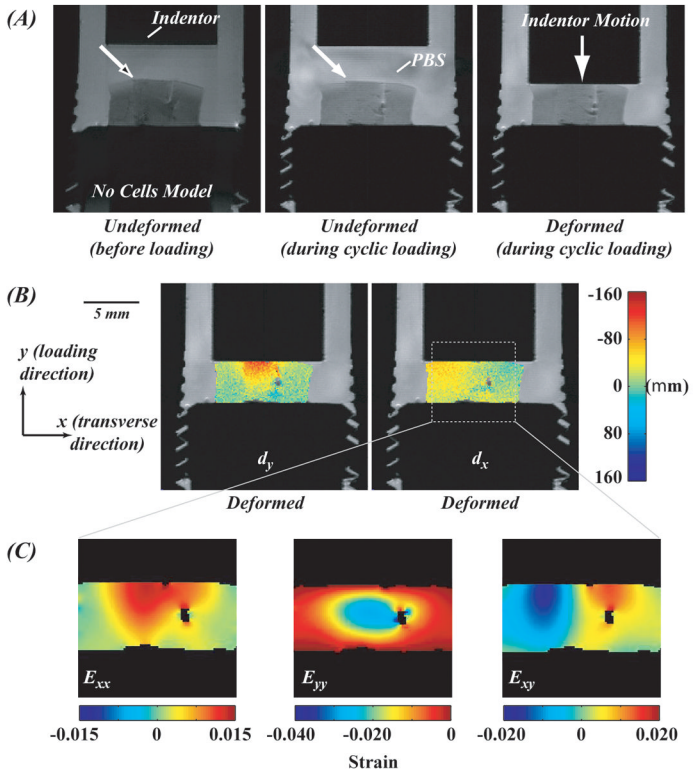

Figure 3.

Displacement and strain fields in a cartilage-agarose construct (*no cells model*) during cyclic loading were heterogeneous. Displacements in the loading direction (d_y) varied with spatial position and approached −160 μm in some tissue regions. The magnitude of deformation *(B and C)* was attributed to the lack of integration at the agarose-cartilage boundary and the height of the hydrogel construct compared to the surrounding cartilage in the undeformed state (solid white arrows).

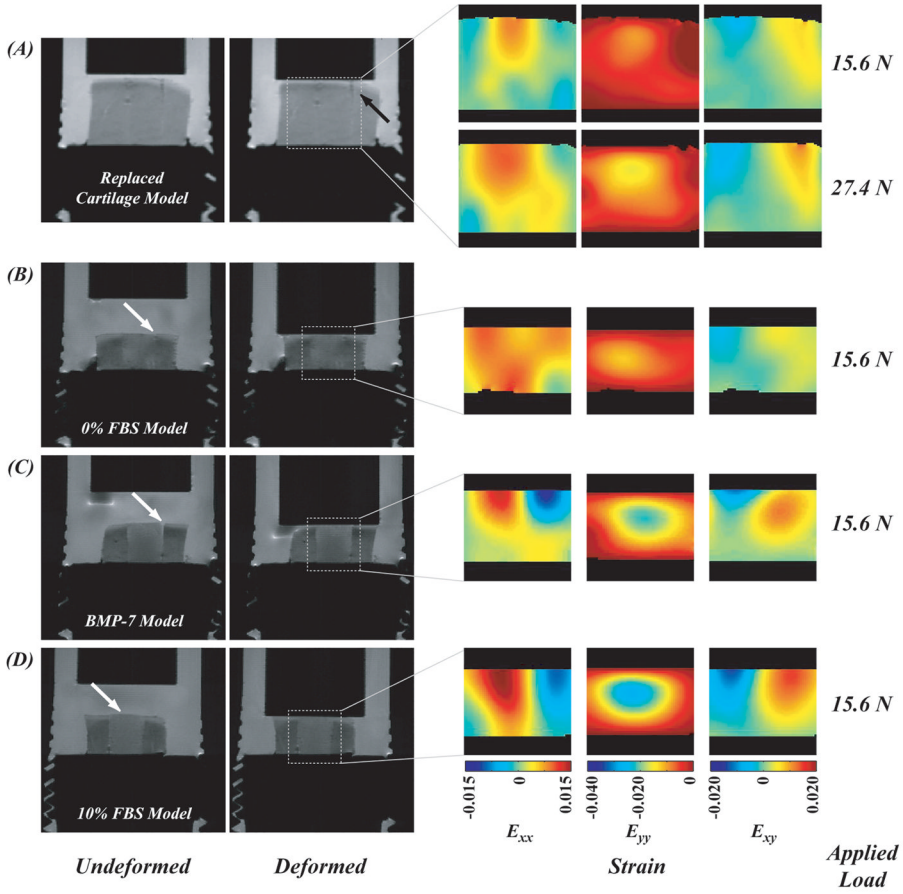

Figure 4.

Strain fields in the tissue-engineered constructs during cyclic loading were nonuniform. Strains in the loading direction (E_{yy}) varied with spatial position and approached −0.040 typically within the agarose construct. The magnitude of deformation was attributed to the lack of integration at the agarose-cartilage boundary and the height of the hydrogel construct compared to the surrounding cartilage in the undeformed state (solid white arrows) (see Discussion). The lack of integration was in particular pronounced with increasing applied load in the magnitude of E_{xy} in *(A)*.

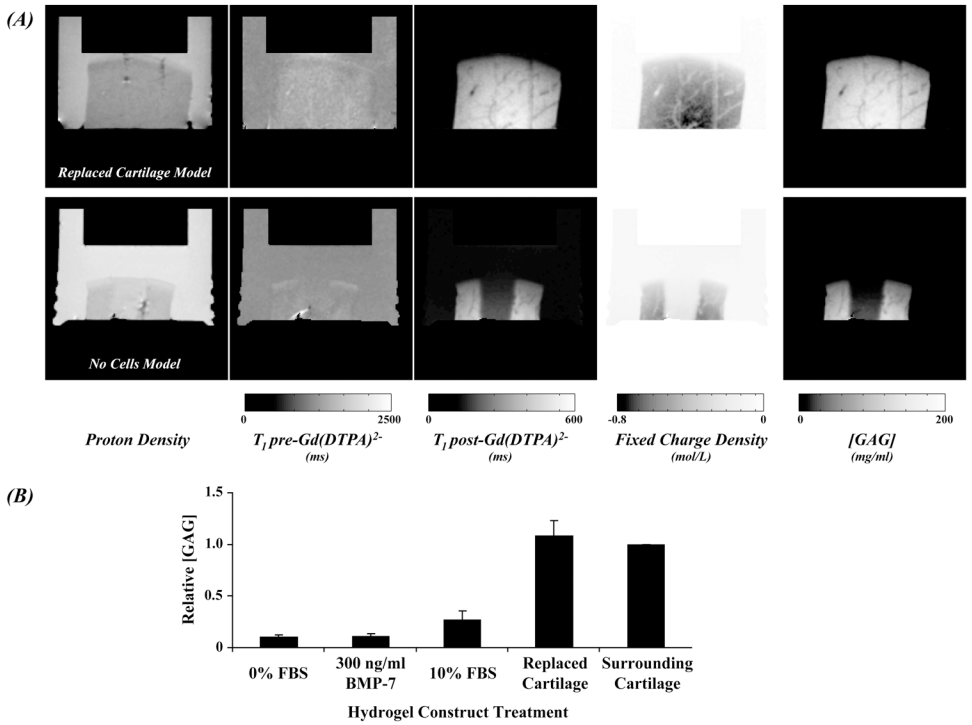

Figure 5.

The spatial variation in [GAG] was determined in the tissue-engineered constructs. T_1 measurements pre- and post-Gd(DTPA)$^{2-}$ were used to compute the fixed charge density and ultimately [GAG] *(A)*. Defect fills with replaced cartilage and agarose containing no cells demonstrate the range observed differences in relative [GAG]. Relative [GAG] computed in the constructs revealed the inability to restore [GAG] in the hydrogel constructs for the culture conditions described herein *(B)*. Importantly, the error bars represent the variation observed within a single sample tested for each treatment.